Fabian Steinmetz and Christian Renner. Resilience against Shipping Noise and Interference in Low-Power Acoustic Underwater Communication. In Proceedings of the OCEANS Conference 2019, Seattle, WA, USA, Oct. 2019

Resilience against Shipping Noise and Interference in Low-Power Acoustic Underwater Communication

Fabian Steinmetz and Christian Renner
Research Group smartPORT
Hamburg University of Technology
Email: {fabian.steinmetz, christian.renner}@tuhh.de

***Abstract*—Underwater Wireless Sensor Networks (UWSNs) and micro Autonomous Underwater Vehicles (μAUVs) enable diverse underwater monitoring and service applications; e. g., observation of water quality or identification of pollution sources. Reliable underwater communication for data transmission between sensors, μAUVs and base stations is required and typically acoustic. However, vessels and μAUVs produce noise, disturbing the acoustic data transmission. Additionally, in networks there is potentially a risk of packet interference. This paper discusses the resilience against noise and interference of low-power acoustic underwater modems in a network. We used the smartPORT Acoustic Underwater Modem (AHOI modem) to analyze signal processing and modulation schemes in a concrete case. The AHOI modem modem is a small, low-power and low-cost modem, which was developed for UWSNs and integration into μAUVs. Based on our findings, we evaluate the resilience in simulations and through real-world experiments in a marina. In general, the results are useful to design and simulate low-power acoustic underwater communication.**

I. Introduction

Underwater monitoring and service applications are drawing considerable attention. For example, in the year 2017, over 80 % of the international cargo was transported by ships (global trade by volume in [1]). To provide efficient progress, the port infrastructure plays an important role. During the last years, there has been a growing interest in robotic-aided services with the help of Autonomous Underwater Vehicles (AUVs), e. g., Robotic Vessels as-a-Service (RoboVaaS) [2], and Internet of Things (IOT) solutions, e. g., UWSNs [3], for ports and marinas. UWSNs can be used to monitor the port area, measure biological parameters, and detect hazards. Examples are the research project HydroNode [4] and the industrial harbor monitoring network system in [5]. μAUVs such as HippoCampus [6] or Vertex AUV [7] can extend the network as mobile nodes or enable mobiles services, e. g., swarm-based data aggregation [8] or sensor polling [9].

In all cases, reliable underwater communication is a major requirement. Due to the strong attenuation of the electromagnetic wave in the water, most underwater modems use an acoustic communication, e. g., [10]–[14]. Typically, UWSNs or μAUVs require communication ranges in a few hundred meters, and the modems must be cheap, small and low-power devices. Based on the requirements, these modems have a limited amount of computational power and use light-weight data modulation algorithms.

Many applications are located in ports and rivers and include several devices. Ships and AUVs produce acoustic noise, which could disturb acoustic communication. Additionally, in a network of acoustic modems, packet collisions can occur, when several modems transmit concurrently. In both cases, resilience against shipping noise and interference is mandatory to provide a stable communication link between the μAUVs, sensor nodes or a base station.

A preliminary simulation study with the AHOI modem [15] was already presented in [16], [17]. This paper extends the existing simulations with shorter distances to the noise sources (higher noise level at the receiver), an AUV noise simulation, additional interference combinations, and a real-world evaluation. The AHOI modem represents a large population of similar low-power acoustic underwater modems. In [16] the resilience tests were used to simulate the modem behavior in DESERT [18], a simulator for underwater networks based on ns2. Adapted from the measured communication performance, new Media Access Control (MAC) protocols can be developed and simulated.

Furthermore, there exist several techniques and lightweight algorithms to improve resilience against noise and interference. Opposed to the previous simulations with the AHOI modem's default setup, this paper includes a comparison between different communication techniques. Based on that, an appropriate choice of parameters can be archived.

A. Contributions

In the following sections, we investigate different signal processing and modulation approaches to enhance the stability against noise and interference. For the implementation on low-power and low-cost modems, algorithms with a lightweight computational complexity are required. Afterwards, we discuss noise sources and interference and simulate their influence on communication reliability. Typically, low-power and low-cost acoustic underwater modems are used for UWSNs or AUVs in harbors, lakes, or rivers. Thereby, noise sources are ships or the self-produced noise by the AUV. We use the AHOI modem to explain and test our findings. In general, the results are useful for Frequency Shift Keying (FSK)-based low-power acoustic underwater communication. At last, we validate our simulation results with an extensive real-world evaluation.

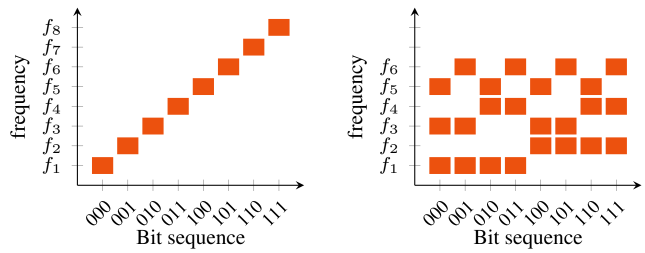

(a) 8-FSK (b) OFDM-BFSK

Figure 1: FSK-based methods to modulate 3 bit (bit sequence) to a single symbol. An 8FSK requires the frequencies f_1 to f_8. Opposed to that, three BFSK on different carriers modulates the sequence with f_1 to f_6. In the case of orthogonality, it is called OFDM-BFSK.

II. Modulation and Transmission

This section introduces FSK-based modulation and demodulation for underwater communication. Due to space constraints, the following section explains selected techniques. For more information, the reader is referred to standard reference works in communication engineering, e. g., [19].

Due to the high attenuation of electromagnetic waves in water, most of the underwater communication uses acoustic waves. Opposed to electromagnetic waves, which travel with $3 \times 10^8\,\mathrm{m/s}$, acoustic waves are much slower and travels underwater with $1500\,\mathrm{m/s}$. When the acoustic wave propagates through the water, the signal is attenuated. The path loss depends on frequency and distance. As a result of damping of higher frequencies (cf. Sect. V-A) and stronger acoustic noise at lower frequencies (cf. Sect. III-A), most of the acoustic underwater modems use frequencies between $10\,\mathrm{kHz}$ and $100\,\mathrm{kHz}$ (e. g., [10]–[14]).

A. Modulation

There exist different modulation methods, e. g., Amplitude Shift Keying (ASK), Frequency Shift Keying (FSK) and Phase Shift Keying (PSK). In the case of an ASK-based transmission, the data modulates the amplitude and in the case of PSK the phase of a transmission wave. Opposed to that, a FSK-based transmission modulates data in different frequencies. A large amount of acoustic underwater modems use a PSK or FSK-based transmission (e. g., FSK-based [12]–[14] and PSK-based [12]) due to the stability against noise and multipath propagation. This paper focuses on the FSK-based underwater transmission, which is implemented on the AHOI modem.

A Binary Frequency Shift Keying (BFSK) uses two frequencies f_1 and f_2 two represent a single bit $B \in \{0, 1\}$. The transmitted symbol $s(t)$ is

$$s(t) = \begin{cases} \sin(2\pi f_1 t) & \text{for } B = 0 \\ \sin(2\pi f_2 t) & \text{for } B = 1 \end{cases} \quad t \in (0, T) \tag{1}$$

with the symbol length T. Another common description is a frequency modulation in the base-band and afterwards a frequency shift to the carrier frequency f_0 in the transmission-band. To enhance the data rate, a M-ary Frequency Shift Keying (MFSK) uses M frequencies (M is usually a power of 2) to transmit $N = \log_2(M)$ bits per symbol. As an example, Fig. 1a depicts a 8-FSK with 3 bits per symbol, which uses the frequencies f_1 up to f_8. Typically with an equidistant frequency spacing of Δf. The well-known JANUS standard for acoustic underwater communication based on a BFSK [20].

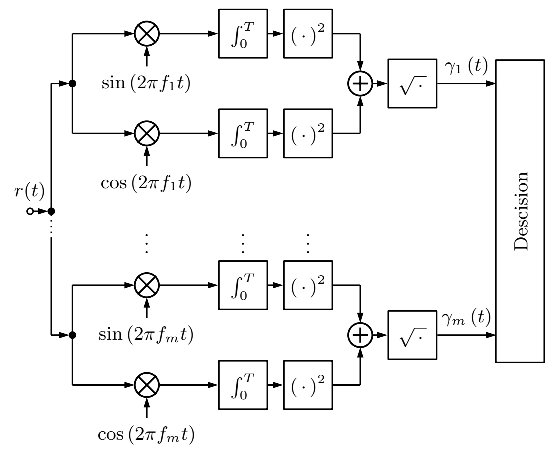

Figure 2: Non-coherent receiver with the received signal $r(t)$ and the frequencies f_1 to f_m. The square root before the decision stage can be neglected in the case of a hard decision.

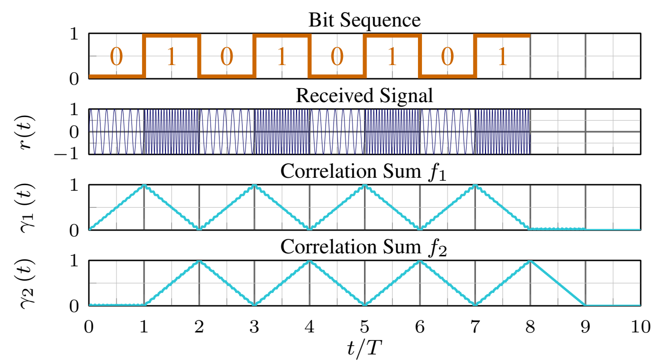

Figure 3: Bit sequence, the resulting BFSK modulated signal using Eq. (1) (received signal is equal to the transmitted signal in this case), and the input to the decision stage $\gamma_1(t)$ and $\gamma_2(t)$ (cf. Fig. 2).

Opposed to the MFSK, it is feasible to add multiple BFSK with different frequencies in order to transmit more than a single bit per symbol. Figure 1b shows an example to transmit 3 bits per symbol with the summation of three BFSK modulated symbols. In the case of orthogonality between the carrier frequencies, this method is known as Orthogonal Frequency-Division Multiplexing (OFDM).

To transmit N bits per symbol, the BFSK with OFDM requires $2N$ and a MFSK 2^N different frequencies. The BFSK with OFDM is more frequency efficient. On the other hand, the MFSK has a higher power per frequency compared to the BFSK with OFDM, when the transmission power is constant. Hence, the MFSK is more stable against additive white noise.

Simple and computationally light-weight detection methods are coherent and non-coherent detection. Figure 2 depicts a non-coherent receiver structure with the received signal $r(t)$

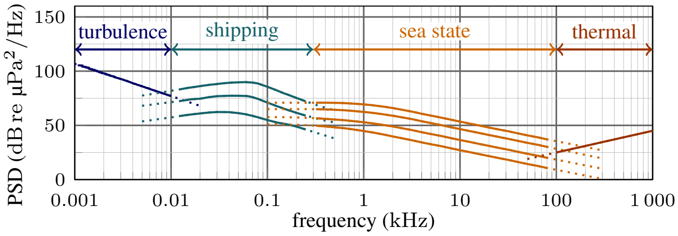

(a) Environmental ambient noise

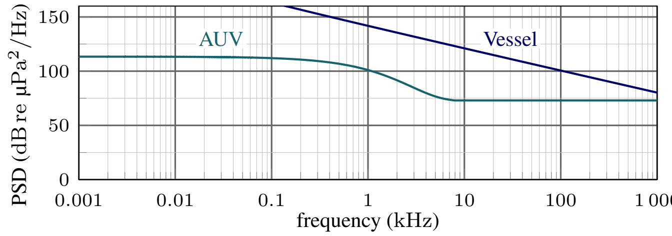

(b) Emitted noise from a ship and an AUV

Figure 4: Environmental ambient noise and emitted noise from a ship and an AUV. The ambient noises are calculated with the equations and tables from [21], [22]. Far shipping noise is depicted with different shipping activity levels (heavy, moderate and light far shipping activity) and sea state noise for wind speeds of 0-1 knot, 4-6 knots, 11-16 knots, and 28-40 knots. The ship and AUV PSDs are derived with the equations presented in [23] for an 180 m cargo vessel with 15 knots and Bluefin Robotics AUV [24].

and the frequencies f_1 to f_m. The non-coherent receiver enables detection with phase-shifted signals, in contrast to the coherent receiver, which multiplies the received signal with a sine instead of sine and cosine.

The decision stage (cf. Fig. 2) decides for the highest input(s) (depending on the modulation scheme) per symbol. Figure 3 gives an example, a bit sequence 01010101 is BFSK-modulated to the frequencies f_1 and f_2. The correlation sums $\gamma_1(t)$ and $\gamma_2(t)$ are the decision stage input signals and the decision stage chooses for each bit the higher correlation sum to estimate the transmitted bit.

B. Frequency Hopping and Spreading

In the case of a single propagation path, defined as Line-of-Sight (LOS), the demodulation of the transmitted signal is simple (cf. Fig. 3). However, the acoustic shallow-water channel is one of the most challenging transmission channels with strong multipath propagation [25]. The transmitted signal is reflected at the water surface and other objects, e. g., bottom, quay walls, plants and ships, which leads to multiple propagation paths, defined as Non-Line-of-Sight (NLOS) propagation paths. Due to the multipath propagation, the channel is frequency selective, and received signals are distorted with inter- and intra-symbol interference.

To deal with these challenges, different techniques can be used. At first, frequency hopping prevents inter-symbol interference and spreads the signals over a larger bandwidth. Frequency-Hopping Spread Spectrum (FHSS) switches the carriers instead of using a single carrier. In addition, to counter frequency cancellations produced by intra-symbol interference, symbol repetitions with different frequencies are a lightweight method. In Sect. IV-C, both methods are explained in more detail based on the modulation of the AHOI modem.

III. Noise and Signal Interference

This section presents acoustic underwater noise and different ship and AUV noise profiles. In addition, interference in underwater networks is discussed. The resilience evaluations are based on the findings in this section.

A. Acoustic Noise

There exist several noise sources. Natural noise sources are ambient noise, e. g., wind, waves and rain, and animal noise, e. g., dolphins and the snapping shrimp [25]. Another important noise source in ports is man-made noise, e. g., ships and sonars. The authors in [21], [22] explain different noise sources and give equations and tables to derive the noise Power Spectral Densities (PSDs). Based on that, the PSDs in Fig. 4a are derived. In the frequency region between 1 Hz and 10 Hz ocean turbulence is the dominant noise source. Far shipping noise dominates the frequencies 10 Hz to 300 Hz and is depicted in Fig. 4a for different shipping activity levels, e. g., light (shipping level 1), moderate (shipping level 4) and heavy (shipping level 7) far shipping activity (cf. [22]). At higher frequencies, the sea state, caused by wind and waves, produces acoustic noise in the region between 300 Hz and 100 kHz. The resulting PSDs are derived for different sea states, defined by wind speeds [21]. Figure 4a shows the acoustic noise for wind speeds of 0-1 knot (sea state 0), 4-6 knots (sea state 1), 11-16 knots (sea state 3), and 28-40 knots (sea state 6). At last, thermal noise affects the region between 100 kHz and 1 MHz.

The previous model includes far shipping noise in the ocean. For acoustic near shipping noise modeling, the authors in [23] presented a detailed analysis of different noise sources, different ships and AUVs. The intensity and frequency of ship noise depend, e. g., on speed and ship length. In addition, an equation is derived to calculate noise PSDs. Two models are depicted in Fig. 4b. At first, a noise model for a 180 m cargo vessel, traveling with a velocity of 15 knots, and the second one for an AUV from Bluefin Robotics [24]. In both cases, the acoustic noise emitted by ship and AUVs have highest PSDs in the lower frequency range.

In comparison between both diagrams in Fig. 4, the emitted acoustic noise by a ship or an AUV is higher than the environmental ambient noise. In harbors or ports, with short distances to ships and AUVs the derived PSDs in Fig. 4b dominate the acoustic background noise.

B. Signal Interference

In UWSNs, multiple sensor nodes (attached to a modem) transmit and receive data. The simplest way is to start a data transmission, as soon as the data is recorded. This concept can lead to packet interference, if several nodes need to use the transmission channel at the same time and packets overlap at the receiver. A more coordinated transmission medium access

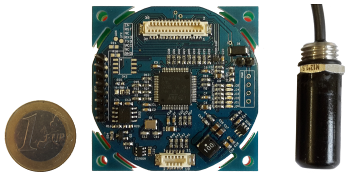

Figure 5: smartPORT Acoustic Underwater Modem (AHOI modem) with an AS-1 hydrophone (and 1-euro coin).

(Carrier Sense Multiple Access, CSMA) is to listen to the channel before the transmission. If the channel is unused, the sender starts the transmission. Opposed to the speed of light in a wireless over-water transmission (using electromagnetic waves), the speed of sound in an underwater scenario is much lower. For short distances, propagation delays are in the millisecond range; e. g., for $150\,\mathrm{m}$ a propagation time of $100\,\mathrm{ms}$ (in contrast to propagation times less than $1\,\mathrm{ns}$ for wireless over-water communication). Additionally, in a network with μAUVs, protocols with time synchronization and a fixed communication time slot for each node, e. g., Time Division Multiple Access (TDMA), are impractical due to the high variation of the propagation time (due to mobility). In sum, media access is a critical point in UWSN, and there is a risk of packet interference. An extensive discussion on UWSN media access can be found in [3].

IV. AHOI - Acoustic Underwater Modem

The AHOI modem is a small, low-power and low-cost acoustic underwater modem (cf. Fig. 5 and [15], [26]), developed to be integrated into UWSNs and μAUVs (e. g., the HippoCampus [6]). The modem consists of three stacked Printed Circuit Boards (PCBs) with an overall size of $50 \times 50 \times 25\,\mathrm{mm}^3$ and approximately €200 component cost. The first PCB includes a CortexM4 microcontroller, power supply and external connections. In addition, the second PCB works as the receiver and involves amplifiers, a Band-Pass (BP) filter and an Analog-to-Digital Converter (ADC). To receive acoustic signals with different signal strength, the amplifier gains are software adjustable (overall amplification between $40\,\mathrm{dB}$ to $96\,\mathrm{dB}$). In the default setup, a software-based automatic gain control is used to adjust the amplifier gains. Finally, the third PCB is the transmission board including a Digital-to-Analog Converter (DAC) and a power amplifier. The power consumption in idle and receive mode is around $300\,\mathrm{mW}$ and $2.1\,\mathrm{W}$ during data transmission with highest amplification. For the acoustic signal reception and transmission, the AHOI modem uses an Aquarian Audio AS-1 hydrophone [27] with a price of ca. €400. In the case of the highest power amplifier level and a transmission in the range between $50\,\mathrm{kHz}$ to $75\,\mathrm{kHz}$, the transmission source level is between 150 to $160\,\mathrm{dB\,re\,\mu Pa}$ @$1\,\mathrm{m}$ with an AS-1 hydrophone.

A. Receiver Design

Before the digitization of the received signal, the signal passes through an analog processing chain (cf. Fig. 6). At first, the signal is pre-amplified to have a higher signal

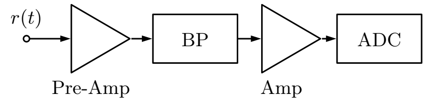

Figure 6: Analog receiving chain. At first, the received signal $r(t)$ from the hydrophone is pre-amplified and passes a BP filter. Afterwards, the signal is amplified again and digitized with an ADC.

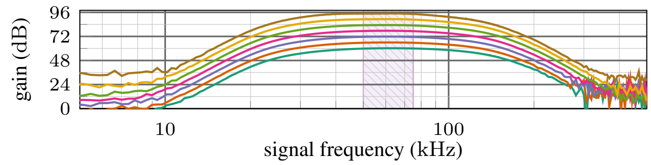

Figure 7: Measured transfer function of the analog receiving signal chain of an AHOI modem. The pre-ampliefier gain was set to $54\,\mathrm{dB}$ and the amplifier gain was adjusted from $6\,\mathrm{dB}$ to $42\,\mathrm{dB}$ in $6\,\mathrm{dB}$ steps (in general $2\,\mathrm{dB}$ is the minimum step width).

level. Afterwards a High-Pass (HP) filter with cut-off frequency $f_c = 50\,\mathrm{kHz}$ reduces signal components with lower frequencies and a Low-Pass (LP) filter with $f_c = 75\,\mathrm{kHz}$ reduces the higher parts. In sum, the HP and LP form a BP filter. Figure 7 shows the receiving characteristic for selected gain steps (analog signal chain between $r(t)$ and ADC in Fig. 6). At last, the signal is digitized with an ADC, using $200\,\mathrm{kHz}$ sampling frequency.

B. Hydrophone Characteristic

The AHOI modem uses a single transducer to receive and to transmit (see Sect. IV). In Fig. 8 the Free-Field Voltage Sensitivity (FFVS) and Transmit Voltage Response (TVR) of the hydrophone are depicted. The FFVS in the range from $1\,\mathrm{kHz}$ to $100\,\mathrm{kHz}$ is almost linear ($\pm 2\,\mathrm{dB}$) and has a sensitivity of $-208\,\mathrm{dBV\,re\,1\mu Pa}$. Opposed to the FFVS, the TVR is highly frequency dependent. During a transmission, the modem compensates the frequency-dependent characteristic.

C. Modulation and Coding

Signal processing is realized in software on the microcontroller, which allows a fast reconfiguration of frequency and coding setups. The communication is packet-based and each packet starts with a preamble to apply a per-packet synchronization. The default setup uses 16 synchronization symbols, followed by a four-symbol Start Frame Delimiter (SFD) to determine the begin of the modulated data. A packet consists of a $6\,\mathrm{Byte}$ header (extended with a $1\,\mathrm{Byte}$ Cyclic Redundancy Check (CRC) checksum) and payload (extended with a $2\,\mathrm{Byte}$ CRC checksum).

The AHOI modem uses an OFDM-BFSK (cf. Fig. 1b) with $N \in \{1, 2, ..., 6\}$ bits per symbol in order to enhance the data rate (compared to a single bit per symbol). According to Sect. II-A, each symbol consists of N superimposed sinusoidal waveforms. The implemented symbol lengths are $T \in \{1.28\,\mathrm{ms}, 2.56\,\mathrm{ms}\}$, resulting in 256 and 512 samples per symbol. To counter frequency- and time-dependent attenuation caused by multipath propagation (cf. Sect. II-B) and to enhance the reliability against noise, each bit is

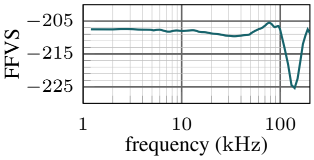

(a) AS-1 as receiver

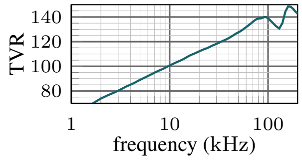

(b) AS-1 as transmitter

Figure 8: Hydrophone characteristics. FFVS in $[\mathrm{dB\,re\,1V/\mu Pa}]$ and TVR in $[\mathrm{dB\,re\,1\mu Pa, 1V@1\,m}]$ of an Aquarian Audio AS-1 [27].

repeated $S \in \{1, 2, 3\}$ times. This mechanism adds redundancy with the price of a lower data rate. At last, FHSS with $H \in \{1, 2, 3\}$ carriers is applied to avoid inter-symbol interference ($H = 1$ means without hopping). Furthermore, the repetition in combination with FHSS distributes the repeated bits over a wider bandwidth. The result is visible in comparison between Fig. 9b and Fig. 9c. In Fig. 9b ($S = 3$, $H = 1$) the bits are repeated on the same frequency. Opposed to that, in Fig. 9c ($S = 3$, $H = 3$) FHSS is applied an the bits are distributed over more frequencies.

The default setup uses $N = 4$ bits per symbol with $T = 2.56\,\mathrm{ms}$ symbol length, a bit repetition of $S = 3$ and $H = 3$ hopping sequence length.

Furthermore, the gross data rate is

$$r_{\text{gross}} = N / \left(S \cdot T \right). \tag{2}$$

In addition, extended Hamming codes are used, which halves the data rate to the net data rate $r_{\text{net}} = 0.5 \cdot r_{\text{gross}}$. In the default setup ($S = 3$, $N = 4$, $T = 2.56\,\mathrm{ms}$), net data rate is $r_{\text{net}} = 260\,\mathrm{bit/s}$ at a bandwidth of $25\,\mathrm{kHz}$. However, the maximum net data rate is currently $r_{\text{net}} = 2.35\,\mathrm{kbit/s}$ for $S = 1$, $N = 6$, $T = 1.28\,\mathrm{ms}$ ($37.5\,\mathrm{kHz}$ bandwidth) and $r_{\text{net}} = 4.7\,\mathrm{kbit/s}$ without Hamming coding.

Figure 9 depicts data packets with $8\,\mathrm{Byte}$ payload and different modulation parameters (default configuration in Fig. 9c). In all cases, the packet starts with a synchronization with 16 preamble symbols and a four-symbol SFD (the synchronization symbols have the same symbol length T). Afterwards, header and payload are transmitted. The packet length and the used frequencies depend on the modulation setup.

At the receiver side, the decision stage (cf. Sect. II-A) combines S bit repetitions ($S > 1$). The firmware involves two different methods (t in $\gamma_m(t)$ is determined with the per-packet synchronization):

1) Choose the bit with the highest correlation sum $\gamma_m(t)$, $m \in \{1, 2, ..., 2S\}$.
2) Add up all correlation sums $\gamma_m(t)$ for a received binary 0 ($m \in \{1, 3, ..., 2S - 1\}$) and a received binary 1 ($m \in \{2, 4, ..., 2S\}$). Choose the bit with the highest value.

The first method enhances resilience against narrow-band frequency cancellations, because the decision is based on a single received frequency. Opposed to that, the second method involves all frequencies and enhances the robustness against noise (equally distributed over the bandwidth). In the default setup the AHOI modem uses the first method.

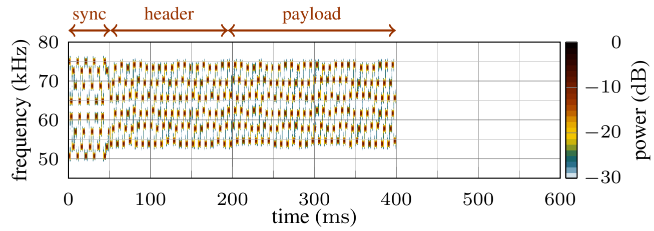

(a) $S = 1$, $N = 2$, $H = 3$, $T = 2.56\,\mathrm{ms}$

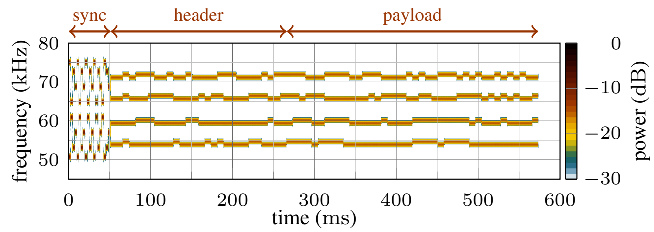

(b) $S = 3$, $N = 4$, $H = 1$, $T = 2.56\,\mathrm{ms}$

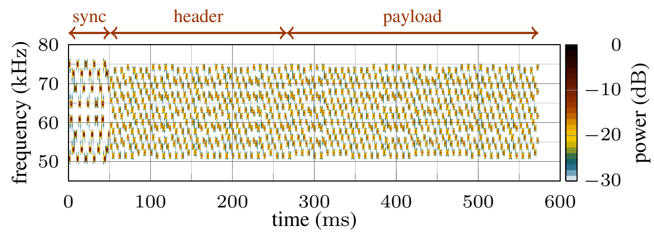

(c) $S = 3$, $N = 4$, $H = 3$, $T = 2.56\,\mathrm{ms}$ (default configuration)

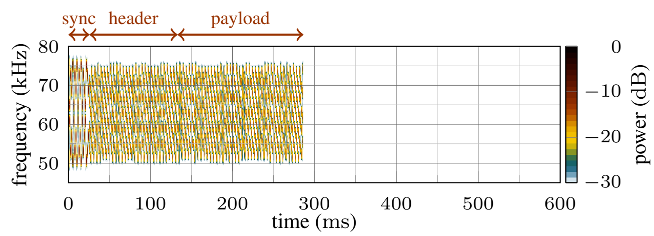

(d) $S = 3$, $N = 4$, $H = 3$, $T = 1.28\,\mathrm{ms}$

Figure 9: Data packets with $8\,\mathrm{Byte}$ payload and different modulation parameters. In all cases, the packet starts with a synchronization with 16 preamble symbols and a four-symbol SFD. Afterwards, header and payload are transmitted.

V. Experimentation Setup

The resilience against shipping noise and packet interference was evaluated via simulation and in a real-world scenario. This section describes the setups for both evaluations.

A. Simulations

A simulation was performed to assess the resilience against ship and AUV noise. The noise for a $180\,\mathrm{m}$ cargo vessel with $15\,\mathrm{knots}$ and an AUV (cf. noise PSDs in Fig. 4b) were generated offline and added to different recorded packets. A single AHOI modem was used to receive the signal, which was generated with an arbitrary signal generator (TiePie Handyscope HS5[1], $200\,\mathrm{kHz}$ sampling). The signal generator simulated the hydrophone voltage response for different PSDs, assuming a frequency independent sensitivity of $-208\,\mathrm{dBV\,re\,1\mu Pa}$ (cf. FFVS in Sect. IV-B).

[1] https://www.tiepie.com/en/usb-oscilloscope, accessed: 2019/08/21

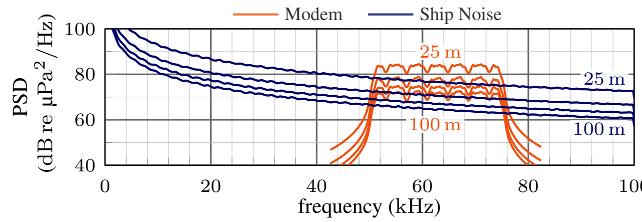

(a) Modem packet and ship noise

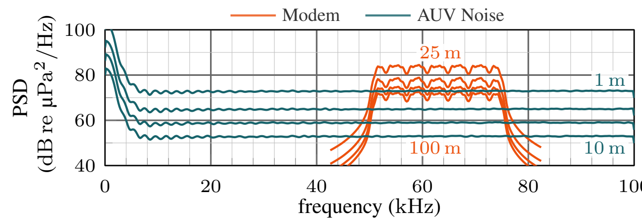

(b) Modem packet and AUV noise

Figure 10: PSDs of the simulated modem signals and additional shipping noise. The PSDs correspond to received signals (packets or noise) with $d_{\text{M}}, d_{\text{ship}} \in \{25\,\text{m}, 50\,\text{m}, 75\,\text{m}, 100\,\text{m}\}$ and $d_{\text{AUV}} \in \{1\,\text{m}, 2.5\,\text{m}, 5\,\text{m}, 10\,\text{m}\}$ distance to the transmitter or noise source. The modem uses the default modulation configuration.

The received signal strength was calculated with the path loss. When the acoustic wave travels through the water, the signal is attenuated. The path loss depends on the frequency f and the distance d (in relation to a reference distance d_0) between sender and receiver. The attenuation is

$$L(d, f) = L_{\text{spr}}(d) + L_{\text{abs}}(d, f) \tag{3}$$

$$= 20 \cdot n \cdot \log_{10}(d/d_0) + (d - d_0) \cdot \alpha(f)\ \text{dB} \tag{4}$$

with spread loss L_{spr} and absorption loss L_{abs}. The path loss exponent n depends on the situation and environment. For a spherical spreading and a free-field assumption, the exponent is $n = 1$. In contrast to spread loss, absorption loss is frequency-dependent. The function $\alpha(f)$ models attenuation in relation to the frequency. Different models are discussed in [21], e.g. the Schulkin and Marsh formula. Assuming test conditions from Sect. V-B, typical absorption losses are less than $3\,\text{dB/km}$ for frequencies up to $100\,\text{kHz}$. Based on that, absorption loss is negligible in small communication distances compared to spread loss; e. g., $L_{\text{spr}}(100\,\text{m}) = 40\,\text{dB}$. Attenuation for short distances can be approximated with

$$L(d) \approx 20 \log_{10}(d/d_0)\,. \tag{5}$$

With the help of Eq. (5) the simulated modem signal and noise PSDs were calculated. Figure 10 shows the PSDs of received packets at the receiver side (neglecting all propagation paths besides LOS) for distances to transmitter $d_{\text{M}} \in \{25\,\text{m}, 50\,\text{m}, 75\,\text{m}, 100\,\text{m}\}$. The modem PSDs in Fig. 10 exhibit the default modulation configuration and an average transmission level of $150\,\text{dB re µPa @1 m}$ (cf. Sect. IV). All evaluations used the same amplification factors.

During the simulations, different noise profiles were added to the packets. The noise profiles were generated in accordance to [23] and are also shown in Fig. 10. In both cases (ship

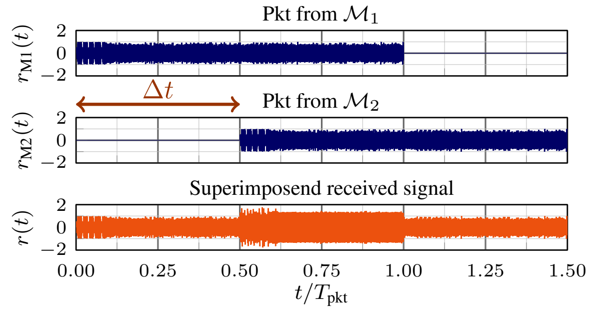

Figure 11: Example for $\Delta t = 0.5 \cdot T_{\text{pkt}}$. The packet (Pkt) from $\mathcal{M}_1$ ($r_{M1}(t)$) received at $t = 0$ and from $\mathcal{M}_2$ ($r_{Mr}(t)$) at $t = \Delta t = 0.5 \cdot T_{\text{pkt}}$. The receiver receives the superimposed signal $r(t) = r_{M1}(t) + r_{M2}(t)$.

and AUV noise), the noise sources were assumed as point-sources and the path loss was calculated with Eq. (5) using distances to the ship $d_{\text{ship}} \in \{25\,\text{m}, 50\,\text{m}, 75\,\text{m}, 100\,\text{m}\}$ and $d_{\text{AUV}} \in \{1\,\text{m}, 2.5\,\text{m}, 5\,\text{m}, 10\,\text{m}\}$ to the AUV. The ship noise was calculated for a $180\,\text{m}$ long cargo vessel (and assumed as a point source), which is larger than d_{ship}. In reality, the ship noise sources are distributed over the ship hull and the received signal level is lower. Opposed to that, AUVs are smaller and the distances d_{AUV} simulates an integration of the receiver into or near to an AUV.

For each combination of ship or AUV noise level and communication signal strength, 500 transmissions were simulated (with $32\,\text{Byte}$ payload per packet) with the default modulation configuration. Afterwards, different modulations were simulated with the lowest Signal to Noise Ratio (SNR) combination ($d_{\text{ship}} = 25\,\text{m}$ and $d_{\text{M}} = 100\,\text{m}$).

In addition to ship and AUV noise, other underwater modems in a network could disturb the transmission (cf. Sect. III-B). To evaluate the effect of packet interference and the resulting Packet Reception Rate (PRR), the same simulation setup was used. Instead of additional simulated noise, a second recorded packet was added to the generator samples. All packets carried $32\,\text{Byte}$ payload and had a signal duration in the default setup of $T_{\text{pkt}} = 1.3\,\text{s}$, including the synchronization symbols. During the simulation two modems ($\mathcal{M}_1$ and $\mathcal{M}_2$) transmitted packets with different delays $\Delta t \in \{-1 \cdot T_{\text{pkt}}, -0.95 \cdot T_{\text{pkt}}, ..., 1 \cdot T_{\text{pkt}}\}$ (T_{pkt} depends on the modulation). The time Δt is the reception time difference between $\mathcal{M}_1$ and $\mathcal{M}_2$ at the receiver side w. r. t. the reception of the packet from $\mathcal{M}_1$. For example, $\Delta t < 0$ means the packet from $\mathcal{M}_2$ arrives before the packet sent by $\mathcal{M}_1$. $|\Delta t| > T_{\text{pkt}}$ is a reception without interference. Figure 11 depicts a graphical interpretation of Δt. The signal strengths of the received packets are similar to the noise test (cf. Fig. 10).

B. Real-World Evaluations

The real-world evaluation took place at the Port of Harburg, a small marina in Hamburg (cf. Fig. 12) on a $50\,\text{m}$ jettie. It was warm and windless day in September 2019. In all evaluations, the hydrophones were placed $1.5\,\text{m}$ under the water surface. In addition, we measured temperature and salinity with a pro-

Figure 12: Test area of our real-world evaluation at a port in Hamburg.

fessional Sea&Sun Technologies CTD-48 probe[2]. The water had a temperature of $19.3\,°\mathrm{C}$ and a salinity of $0.26\,\mathrm{ppt}$. Based on that, the speed of sound was approximately $1480.5\,\mathrm{m/s}$.

A real-world evaluation of the resilience against interference has been carried out due to page limitations. However, a short interference evaluation was already published in [17].

We used an Aquarian Audio AS-1 to produce acoustic noise. Due to the smaller TVR (cf. Sect. IV-B) and higher vessel noise (cf. Fig. 4b) at lower frequencies, the noise was filtered with a HP filter with $f_c = 15\,\mathrm{kHz}$ (the AHOI modem uses the frequencies between $50\,\mathrm{kHz}$ and $75\,\mathrm{kHz}$ in the default setup). The hydrophone with the noise signal was placed with $1\,\mathrm{m}$ distance to the receiver and transmitted the noise of a $180\,\mathrm{m}$ cargo vessel (and assumed as a point source) traveling with $15\,\mathrm{knots}$ and a distance of $d_{\text{ship}} \approx 50\,\mathrm{m}$. The transmitter was placed with $d_{\mathrm{M}} = 50\,\mathrm{m}$ distance to the AHOI modem, which was the receiver. To evaluate lower SNRs with communication distances near to $d_{\mathrm{M}} = 100\,\mathrm{m}$ (evaluation took place on a $50\,\mathrm{m}$ jettie), the transmitted communication signals was $6\,\mathrm{dB}$ damped ($L\,(50\,\mathrm{m}) = 34\,\mathrm{dB}$ and $L\,(100\,\mathrm{m}) = 40\,\mathrm{dB}$, cf. Eq. (5)). The evaluation was done for different modulation setups, which are listed in Table III. Every evaluation 250 packets with $32\,\mathrm{Byte}$ payload were transmitted.

VI. Evaluation

This section presents and discusses the results of the simulation and real world evaluation.

A. Simulations

At first, the resilience of the default modem configuration against ship and AUV noise was evaluated. The AUV noise affected the packet reception in a single case, and in the other cases all transmitted packets were received. The combination $d_{\text{AUV}} = 1\,\mathrm{m}$ and $d_{\mathrm{M}} = 100\,\mathrm{m}$ resulted in $99.8\,\%$ received packets (a single packet was not received). Furthermore, Fig. 13 depicts the results of the shipping noise simulations. In most cases, also the shipping noise did not affect the PRR. However, the setup $d_{\text{ship}} = 25\,\mathrm{m}$ and $d_{\mathrm{M}} = 100\,\mathrm{m}$ resulted in a PRR of $36.2\,\%$. In this case, the noise PSD is significantly higher than the communication signal PSD (cf. Fig. 10a). As a simplification during the simulations, the noise source was assumed as a point source and d_{ship} was smaller than the ship length ($180\,\mathrm{m}$). In general, the ship noise sources are distributed over the ship hull and the received signal level is lower (cf. Sect. V-A). Based on the results, the default setup of the AHOI modem is stable against AUV and shipping noise.

[2]https://www.sea-sun-tech.com/product/multiparameter-probe-ctd-48/, accessed: 2019/08/21

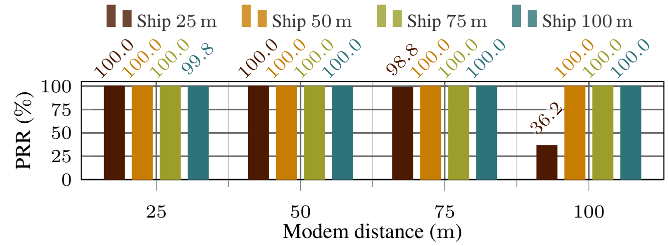

Figure 13: Results of the shipping noise evaluation with the modem's default configuration. The simulated communication and noise distances were $d_{\mathrm{M}}, d_{\text{ship}} \in \{25\,\mathrm{m}, 50\,\mathrm{m}, 75\,\mathrm{m}, 100\,\mathrm{m}\}$. Each combination (respectively bar) 500 packet transmissions were simulated.

Additional, the setup with the lowest PRR in the default configuration ($d_{\text{ship}} = 25\,\mathrm{m}$ and $d_{\mathrm{M}} = 100\,\mathrm{m}$) was used to evaluate the noise resilience of different data modulation settings. Table I lists the number of synchronizations, received SFDs and packets, respectively the PRR, the average corrected bits per Packet Reception (PR), and the PR per received SFD for different bit repetitions S, bits per symbol N, hopping sequence lengths H, symbol lengths T, and detection schemes (best bit and summation of correlations). An extensive explanation of these parameters gives Sect. IV-C. In every setup, 500 packet transmissions were simulated with equal amplification factors (in the default setup the amplification results in a transmission source level of $150\,\mathrm{dB\,re\,\mu Pa\,@1\,m}$ with an AS-1 hydrophone).

The preamble and SFD symbols are independent of the repetitions, number of bits per symbol and hopping scheme. Based on that, preamble and SFD were equal in the first cases with the same symbol length T. Opposed to that, in the last simulation the synchronization symbol length was changed $T = 1.28\,\mathrm{ms}$. Surprisingly, the number of synchronizations and detected SFDs varied between $46.8\,\%$ and $67.4\,\%$ (preamble in Table I), and $28.6\,\%$ and $46.8\,\%$ (SFD in Table I) for the same symbol length and a low SNR[3]. However, the comparison between the number of received packts per detected SFD and the averaged corrected bit errors per received packet gives a benchmark to compare the different modulation schemes. The first setup in Table I lists the default configuration of the AHOI modem. Compared to the default detection algorithm (best bit), the summation of the correlations, enhanced the PR per SFD from $77.4\,\%$ to $82.5\,\%$. In the presence of noise and without NLOS propagation paths, the second detection algorithm was more resilient against shipping noise. On the opposite, less bit repetitions reduced the PR per SFD from $77.4\,\%$ (default, $S = 3$) to $46.8\,\%$ ($S = 2$) and $0\,\%$ ($S = 1$). Based on that, a higher repetition rate increased the probability of a correct data reception. Less bits per symbol enhance the power per transmission frequency and resulted in $100\,\%$ PR per SFD ($N \in \{1, 2, 3\}$) compared to $77.4\,\%$

[3]We are aware of the lag in preamble and SFD detection. In presence of high acoustic noise or strong multipath propagation, the synchronization and SFD detection is the weak spot of our implementation. Currently, we are working on different modulation schemes to improve the per-packet synchronization [28], [29].

Table I: Shipping noise results for different modulation setups and the lowest simulated SNR ($d_{\text{ship}} = 25\,\text{m}$ and $d_{\text{M}} = 100\,\text{m}$). The table lists the number of synchronizations (Preamble), the detected SFDs (SFD), received packets (PRR), the average corrected bits per received packet (av. Err. / PR), and relation between received SFD and packet reception (PR / SFD). Every setup 500 packet transmissions were simulated.

S	N	H	T	Detection	Preamble	SFD	PRR	av. Err. / PR	PR / SFD
Default configuration									
3	**4**	**3**	**2.56 ms**	**best bit**	65.0 %	46.8 %	36.2 %	5.4 bit	77.4 %
Different detection of bit repetitions									
3	4	3	2.56 ms	**sum**	67.4 %	44.6 %	36.8 %	3.7 bit	82.5 %
Bit repetitions									
2	4	3	2.56 ms	best bit	50.0 %	24.8 %	11.6 %	10.0 bit	46.8 %
1	4	3	2.56 ms	best bit	46.8 %	28.6 %	0.0 %	——	0.0 %
Bits per symbol									
3	**3**	3	2.56 ms	best bit	56.0 %	37.8 %	37.8 %	0.3 bit	100.0 %
3	**2**	3	2.56 ms	best bit	65.2 %	40.0 %	40.0 %	0.0 bit	100.0 %
3	**1**	3	2.56 ms	best bit	56.8 %	30.8 %	30.8 %	0.0 bit	100.0 %
Hopping									
3	4	**2**	2.56 ms	best bit	66.0 %	44.2 %	31.4 %	5.5 bit	71.0 %
3	4	**1**	2.56 ms	best bit	63.8 %	42.4 %	35.8 %	4.5 bit	84.4 %
Symbol length									
3	4	3	**1.28 ms**	best bit	68.4 %	21.6 %	0.0 %	——	0.0 %

in the default setup ($N = 4$) and lower average corrected bit errors of $0.3\,\text{bit}$ ($N = 3$) and $0\,\text{bit}$ ($N \in \{1, 2\}$) compared to $5.4\,\text{bit}$ ($N = 4$). Hopping is usually used to counter inter-symbol interference in multipath environments. Unexpectedly, without hopping ($H = 1$) the ratio between PR and received SFD was enhanced. After an inaccurate synchronization, the modem expects the data symbols at false positions in the time domain (symbol frames). Without hopping, these frames can include the following symbol with the same frequency (cf. Sect. IV-C). Opposed to that, in the case of hopping the frames include always symbols with different frequencies (just for an inaccurate synchronization). Assuming an accurate synchronization, hopping did not improve the resilience against shipping noise. At last, a shorter symbol duration ($T = 1.28\,\text{ms}$) resulted in a $0\,\%$ PRR. However, packets were received for smaller transmission distances ($d_{\text{ship}} = 25\,\text{m}$, 500 transmission per setup):

- $d_{\text{M}} = 75\,\text{m} \Rightarrow 24.6\,\%$ PRR ($32.6\,\%$ PR / SFD)
- $d_{\text{M}} = 50\,\text{m} \Rightarrow 90.2\,\%$ PRR ($93.4\,\%$ PR / SFD)
- $d_{\text{M}} = 25\,\text{m} \Rightarrow 98.4\,\%$ PRR ($99.8\,\%$ PR / SFD)

Based on the results, smaller a symbol length reduces the resilience against noise.

The second evaluation simulated packet interference between two modems and different communication distances. Figure 14 depicts the results for $d_{\text{M1}} \in \{25\,\text{m}, 75\,\text{m}\}$ in combination with $d_{\text{M2}} \in \{25\,\text{m}, 50\,\text{m}, 75\,\text{m}, 100\,\text{m}\}$. During the simulation, the overlap time Δt went from $-T_{\text{pkt}}$ to T_{pkt} in $0.05 \cdot T_{\text{pkt}}$ steps.

The results of the evaluation are: (1) Without interference ($|\Delta t| = T_{\text{pkt}}$) all packets from $\mathcal{M}_1$ and $\mathcal{M}_2$ were received. (2) In general, the first packet (w. r. t. the arrival at the receiver) is received, also for the case that the second transmitter is nearer. (3) For the case $\Delta t = 0$ and $d_{\text{M1}} \neq d_{\text{M2}}$ the packet from transmitter with a shorter distance is received. (4) For $\Delta t = 0$ and $d_{\text{M1}} = d_{\text{M2}}$ the PRR goes to zero. (5) For some combinations, the PRR from the first received packet (in all cases, the first received modem had a larger distance than the second one) goes to zero. In these cases, the signals had a frequency cancellation (cf. [17]). Based on the simulation, the default configuration of the AHOI modem is resilient against interference in most cases. The resilience is independent of the packet overlap and depends on frequency cancellations between the packets.

Due to space constrains, the setup $d_{\text{M1}} = 25\,\text{m}$, $d_{\text{M2}} = 50\,\text{m}$ was used to evaluate the resilience against interference of different data modulation settings. Table II lists overall ($\Delta t \in \{-1 \cdot T_{\text{pkt}}, -0.95 \cdot T_{\text{pkt}}, ..., 1 \cdot T_{\text{pkt}}\}$) PRRs for $\mathcal{M}_1$ and $\mathcal{M}_2$. The first row (default configuration) is the summation from the results in Fig. 14a ($d_{\text{M2}} = 50\,\text{m}$).

Based on the results for different modulation schemes, the default setup has a proper resilience against interference. The second detection algorithm of bit repetitions and the configurations with less bit repetitions had approximately the same PRRs. Surprisingly, for a bit repetition of $S = 2$ the PRR from $\mathcal{M}_2$ was $40.3\,\%$ (compared to $34.3\,\%$). The overlap time Δt was calculated w. r. t. the packet length. Different time steps could avoid a frequency cancellation in a single time step. A smaller frequency hopping length H results in less used frequencies and enhance the probability of a frequency overlap between $\mathcal{M}_1$ and $\mathcal{M}_2$ at the same time. The PRRs from $\mathcal{M}_2$ with a lower received signal level were reduced for shorter hopping lengths. Based on that, hopping improves the resilience against packet interference. At last, the resilience of shorter symbols was evaluated. The overall PRR from $\mathcal{M}_1$ was

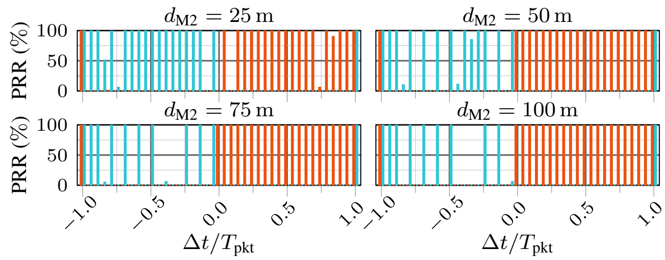

(a) Distance to $\mathcal{M}_1$: $d_{\mathrm{M1}} = 25\,\mathrm{m}$

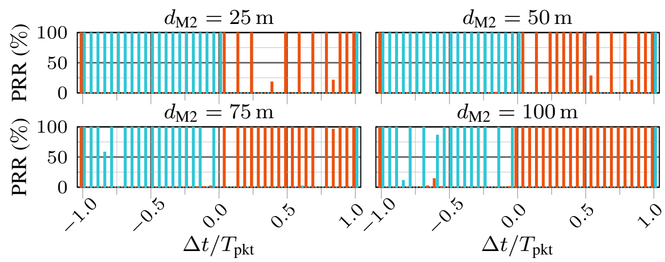

(b) Distance to $\mathcal{M}_1$: $d_{\mathrm{M1}} = 75\,\mathrm{m}$

Figure 14: Packet interference simulation between $\mathcal{M}_1$ and $\mathcal{M}_2$. The time Δt is defined in Fig. 11. The received signal was calculated w. r. t. $d_{\mathrm{M1}} \in \{25\,\mathrm{m}, 75\,\mathrm{m}\}$ and $d_{\mathrm{M2}} \in \{25\,\mathrm{m}, 50\,\mathrm{m}, 75\,\mathrm{m}, 100\,\mathrm{m}\}$. Red bars show the PRRs from $\mathcal{M}_1$ and blue bars from $\mathcal{M}_2$.

increased and from $\mathcal{M}_2$ decreased. Compared to the default setup, $\mathcal{M}_1$ distorts the reception from $\mathcal{M}_2$ for $\Delta t < 0$. Hence, more packages from $\mathcal{M}_1$ were received.

B. Real-World Evaluations

During the real-world evaluations resilience against shipping noise was evaluated. Transmitter and receiver were placed with $d_{\mathrm{M}} = 50\,\mathrm{m}$ distance, and another hydrophone with $1\,\mathrm{m}$ distance to the receiver generated shipping noise. Opposed to the simulations, additional multipath propagation distorted the received packet. The results lists Table III.

At first, the default configuration was tested. During the first evaluations ($d_{\mathrm{M}} = 50\,\mathrm{m}$, with and without noise) the PRRs were $99.2\,\%$, respectively $100\,\%$. However, at the second communication distance of $d_{\mathrm{M}} = 100\,\mathrm{m}$ ($50\,\mathrm{m}$ physical distance and additional $6\,\mathrm{dB}$ attenuation) PRRs were reduced to $90.8\,\%$ (without noise) and $41.2\,\%$ (with noise). Similar to Sect. VI-A, in the most cases the synchronization or SFD detection failed. The ratios between PR and detected SFD were $99.2\,\%$, respectively $100\,\%$. Hence, the default modulation was stable against shipping noise. Due to multipath propagation and additional noise in the real-world evaluation, the PRR reduction (based on failed synchronizations and SFD detection) occurred also for the combination $d_{\mathrm{M}} = 50\,\mathrm{m}$, $d_{\mathrm{ship}} = 100\,\mathrm{m}$ opposed to the simulations.

Afterwards, configurations with a different detection of bit repetitions, fewer repetitions ($S = 2$), and less bits per symbol ($N = 2$) were used. Comparable to the simulations, fewer repetitions significantly reduced the PRRs (also during the evaluations without noise). Opposed to that, less bits per symbol enhance the power per frequency, which resulted in more correct receptions. Due to multipath propagation, a reduction of the hopping length to $H = 2$ resulted in the

Table II: Interference results for different modulation setups. The table lists overall ($\Delta t \in \{-1 \cdot T_{\mathrm{pkt}}, -0.95 \cdot T_{\mathrm{pkt}}, ..., 1 \cdot T_{\mathrm{pkt}}\}$) PRRs for $\mathcal{M}_1$ ($d_{\mathrm{M1}} = 25\,\mathrm{m}$) and $\mathcal{M}_2$ ($d_{\mathrm{M2}} = 50\,\mathrm{m}$). For every overlap Δt, modem, and modulation setup, 100 packets were transmitted.

S	N	H	T	Detection	PRR $\mathcal{M}_1$	PRR $\mathcal{M}_2$
Default configuration						
3	**4**	**3**	**2.56 ms**	**best bit**	53.7 %	34.3 %
Different detection of bit repetitions						
3	4	3	2.56 ms	**sum**	51.9 %	35.2 %
Bit repetitions						
2	4	3	2.56 ms	best bit	53.7 %	40.3 %
1	4	3	2.56 ms	best bit	53.7 %	35.5 %
Bits per symbol						
3	**3**	3	2.56 ms	best bit	53.7 %	35.5 %
3	**2**	3	2.56 ms	best bit	55.0 %	38.1 %
3	**1**	3	2.56 ms	best bit	53.1 %	36.6 %
Hopping						
3	4	**2**	2.56 ms	best bit	53.7 %	26.8 %
3	4	**1**	2.56 ms	best bit	53.7 %	10.0 %
Symbol length						
3	4	3	**1.28 ms**	best bit	63.5 %	24.3 %

lowest PRR per setup. Surprisingly, a shorter symbol duration of $T = 1.28\,\mathrm{ms}$ had the best PRR per setup. In this specific setup, the synchronization and SFD detection worked much better compared to the default configuration. However, this depends on the situation, e. g., the arrival of the NLOS paths.

In sum, the real-world evaluation confirmed the simulations from Sect. VI-A. Opposed to the simulations with a single propagation path, additional paths distort the reception and lowered the PRRs. However, the behavior and the findings were the same.

VII. Conclusion

We showed with simulations and real-world evaluations that the default data modulation of the AHOI modem is resilient against ship and AUV noise in most cases. In addition, we analyzed packet interference with simulations. In many cases, the modem is resilient against packet interference.

Furthermore, different modulation schemes were tested to enhance the resilience against noise and interference. Compared to the default modulation setup, other configurations enhance resilience. However, these configurations come with the cost of a lower data rate.

Based on our findings, it will be possible to choose modulations for UWSNs or swarms of μAUVs equipped with our AHOI modem. Additional, our evaluations are useful to simulate the AHOI modem's behavior in network simulation tools to develop new MAC protocols.

Acknowledgment

This work has been partially supported by the German Federal Ministry for Economic Affairs and Energy (BMWi, FKZ 03SX463C), and ERA-NET Cofund MarTERA (contract 728053).

Table III: Real world evaluation results with and without shipping noise. The evaluation was done for $d_{\mathrm{M}} = 50\,\mathrm{m}$ and $d_{\mathrm{M}} = 100\,\mathrm{m}$ ($50\,\mathrm{m}$ physical distance and $6\,\mathrm{dB}$ attenuation at the transmitter, cf. Sect. V-B). In the case of shipping noise, another hydrophone produced acoustic noise, which was equal to a $180\,\mathrm{m}$ cargo vessel traveling with $15\,\mathrm{knots}$ and a distance of $d_{\mathrm{ship}} \approx 50\,\mathrm{m}$. The table lists the received packets (PRR) and relation between received SFD and packet reception (PR / SFD). For every setup 250 packets were transmitted.

S	N	H	T	Detection	$d_{\mathrm{M}} = 50\,\mathrm{m}$ without noise		$d_{\mathrm{M}} = 50\,\mathrm{m}$ $d_{\mathrm{ship}} = 50\,\mathrm{m}$		$d_{\mathrm{M}} = 100\,\mathrm{m}$ without noise		$d_{\mathrm{M}} = 100\,\mathrm{m}$ $d_{\mathrm{ship}} = 50\,\mathrm{m}$	
					PRR	PR / SFD	PRR	PR / SFD	PRR	PR / SFD	PRR	PR / SFD
Default configuration												
3	**4**	**3**	**2.56 ms**	**best bit**	99.2 %	99.6 %	100.0 %	100.0 %	90.8 %	100.0 %	41.2 %	99.0 %
Different detection of bit repetitions												
3	4	3	2.56 ms	**sum**	98.8 %	100.0 %	100.0 %	100.0 %	100.0 %	100.0 %	64.8 %	100.0 %
Bit repetitions												
2	4	3	2.56 ms	best bit	60.4 %	63.4 %	23.6 %	25.2 %	63.6 %	65.4 %	6.4 %	7.5 %
Bits per symbol												
3	**2**	3	2.56 ms	best bit	96.0 %	100.0 %	92.8 %	100.0 %	92.8 %	100.0 %	35.2 %	100.0 %
Hopping												
3	4	**2**	2.56 ms	best bit	29.6 %	30.0 %	14.4 %	14.5 %	10.4 %	11.0 %	0.0 %	0.0 %
Symbol length												
3	4	3	**1.28 ms**	best bit	99.6 %	100.0 %	100.0 %	100.0 %	100.0 %	100.0 %	89.2 %	91.7 %

References

[1] United Nations, "Review of Maritime Transport 2018," in *United Nations Conf. on Trade & Development (UNCTAD)*, 2018.

[2] A. Signori, F. Steinmetz, F. Campagnaro, D. Zordan, M. Zorzi, and C. Renner, "Poster: Underwater Communications for the Robotic Vessels as-a-Servic Project," in *13th ACM Int. Conf. on Underwater Networks & Systems (WUWNet)*, Shenzhen, China, 2018.

[3] J. Heidemann, M. Stojanovic, and M. Zorzi, "Underwater Sensor Networks: Applications, Advances, and Challenges," *Philosophical Transactions of the Royal Society–A*, vol. 370, no. 1958, pp. 158–175, 2012.

[4] D. Pinto, S. S. Viana, J. A. M. Nacif, L. F. M. Vieira, M. A. M. Vieira, A. B. Vieira, and A. O. Fernandes, "HydroNode: A Low Cost, Energy Efficient, Multi Purpose Node for Underwater Sensor Networks," in *37th IEEE Conf. on Local Computer Networks*, Clearwater, FL, USA, 2012.

[5] NEC Corparation, "Harbor monitoring network system," https://www.nec.com/en/global/solutions/safety/critical_infra/pdf/harbormonitoring_01.pdf, ac.: 2019/06/18.

[6] A. Hackbarth, E. Kreuzer, and E. Solowjow, "HippoCampus: A Micro Underwater Vehicle for Swarm Applications," in *IEEE/RSJ Int. Conf. on Intelligent Robots and Systems (IROS)*, Hamburg, Germany, 2015.

[7] Hydromea, "Vertex AUV System Overview," http://hydromea.com/vertex_brochure.pdf, ac.: 2019/08/13.

[8] C. Isokeit, B. Meyer, and E. Maehle, "Cooperative Swarm Behaviour For In Situ Underwater Environmental Measurements," in *MTS/IEEE OCEANS Conf. & Exposition (OCEANS)*, Aberdeen, Schottland, 2017.

[9] A. Signori, F. Campagnaro, D. Zordan, F. Favaro, and M. Zorzi, "Underwater Acoustic Sensors Data Collection in the Robotic Vessels as-a-Service Project," in *MTS/IEEE OCEANS Conf. & Exposition (OCEANS)*, Marseille, France, 2019.

[10] Evologics GmbH, "Underwater Acoustic Modems," http://www.evologics.de/en/products/acoustics/, ac.: 2019/08/13.

[11] Teledyne Benthos, "ATM-900 Series," http://www.teledynemarine.com/Lists/Downloads/Benthos_ATM-900_Brochure.pdf, ac.: 2019/08/13.

[12] E. Gallimore, J. Partan, I. Vaughn, S. Singh, J. Shusta, and L. Freitag, "The WHOI Micromodem-2: A Scalable System for Acoustic Communications and Networking," in *MTS/IEEE OCEANS Conf. & Exposition (OCEANS)*, 2010.

[13] G. Cario, A. Casavola, M. Lupia, and C. Rosace, "SeaModem: A Low-Cost Underwater Acoustic Modem for Shallow Water Communication," in *MTS/IEEE OCEANS Conf. & Exposition (OCEANS)*, 2015.

[14] B. Benson, Y. Li, R. Kastner, B. Faunce, K. Domond, D. Kimball, and C. Schurgers, "Design of a Low-Cost, Underwater Acoustic Modem for Short-Range Sensor Networks," in *MTS/IEEE OCEANS Conf. & Exposition (OCEANS)*, Sydney, Australia, 2010.

[15] C. Renner and A. J. Golkowski, "Acoustic Modem for Micro AUVs: Design and Practical Evaluation," in *11th ACM Int. Conf. on Underwater Networks & Systems (WUWNet)*, Shanghai, China, 2016.

[16] F. Campagnaro, F. Steinmetz, A. Signori, D. Zordan, C. Renner, and M. Zorzi, " Data Collection in Shallow Fresh Water Scenarios with Low-Cost Underwater Acoustic Modems ," in *5th Int. Conf. & Exhibition on Underwater Acoustics (UACE)*, Hersonissos, Crete, Greece, 2019.

[17] F. Steinmetz and C. Renner, "Resilience against shipping noise and interference of the ahoi acoustic underwater modem," in *18th GI/ITG KuVS Fachgespräch "Sensornetze" (FGSN)*, Magdeburg, Germany, 2019.

[18] F. Campagnaro, R. Francescon, F. Guerra, F. Favaro, P. Casari, R. Diamant, and M. Zorzi, "The DESERT underwater framework v2: Improved capabilities and extension tools," in *3th IEEE Underwater Communications and Networking Conference (UComms)*, Lerici, Italy, 2016.

[19] S. Haykin and M. Moher, *Communication Systems 5th Ed.* Wiley, 2009.

[20] K. McCoy, B. Tomasi, and G. Zappa, "Janus: the genesis, propagation and use of an underwater standard," in *European Conf. on Underwater Acoustics (ECUA)*, Instanbul, Turkey, 2010.

[21] R. J. Urick, *Principles of Underwater Sound 3rd Ed.* Peninsula, 1996.

[22] R. P. Hodges, *Underwater Acoustics: Analysis, Design and Performance of Sonar*. John Wiley & Sons Ltd., 2010.

[23] E. Coccolo, F. Campagnaro, A. Signori, F. Favaro, and M. Zorzi, "Implementation of AUV and Ship Noise for Link Quality Evaluation in the DESERT Underwater Framework," in *13th ACM Int. Conf. on Underwater Networks & Systems (WUWNet)*, Shenzhen, China, 2018.

[24] General Dynamics, "Bluefin SandShark UUV," https://gdmissionsystems.com/products/underwater-vehicles/bluefin-sandshark-autonomous-underwater-vehicle, ac.: 2019/08/13.

[25] M. Stojanovic and J. Preisig, "Underwater acoustic communication channels: Propagation models and statistical characterization," *IEEE Communications Magazine*, vol. 47, no. 1, pp. 84–89, 2009.

[26] J. Heitmann, L. Bublitz, T. Kortbrae, and C. Renner, "Evolution of an Acoustic Modem for Micro AUVs," in *16th GI/ITG KuVS Fachgespräch "Sensornetze" (FGSN)*, Hamburg, Germany, 2017.

[27] Aquarian Audio & Scientific, "AS-1 Hydrophone," http://www.aquarianaudio.com/as-1-hydrophone.html, ac.: 2019/05/27.

[28] J. Heitmann, F. Steinmetz, and C. Renner, "A case for chirp modulation for low-power acoustic communication in shallow waters," in *17th GI/ITG KuVS Fachgespräch "Sensornetze" (FGSN)*, Braunschweig, Germany, 2018.

[29] F. Steinmetz, J. Heitmann, and C. Renner, "A Practical Guide to Chirp Spread Spectrum for Acoustic Underwater Communication in Shallow Waters," in *13th ACM Int. Conf. on Underwater Networks & Systems (WUWNet)*, Shenzhen, China, 2018.